Nano Energy (2015) 12, 314–321

Available online at www.sciencedirect.com

ScienceDirect

journal homepage: www.elsevier.com/locate/nanoenergy

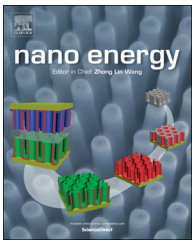

RAPID COMMUNICATION

Improved stability of nano-Sn electrode with high-quality nano-SEI formation for lithium ion battery

KwangSup Eom[a,*], Jaehan Jung[b], Jung Tae Lee[b], Valentin Lair[a], Tapesh Joshi[a], Seung Woo Lee[c], Zhiqun Lin[b], Thomas F. Fuller[a]

[a]*School of Chemical & Biomolecular Engineering, Center for Innovative Fuel Cell and Battery Technologies, Georgia Institute of Technology, Atlanta, GA 30332, USA*
[b]*School of Materials Science and Engineering, Georgia Institute of Technology, Atlanta, GA 30332, USA*
[c]*The George W. Woodruff School of Mechanical Engineering, Georgia Institute of Technology, Atlanta, GA 30332, USA*

Received 5 November 2014; accepted 29 December 2014
Available online 7 January 2015

KEYWORDS
Li ion batteries;
Nano-Sn electrode;
High stability;
Solid electrolyte interphase;
Fluoro-ethylene carbonate

Abstract
Sn materials offer high theoretical capacities in lithium ion batteries, but they must have good cycling stability and high rate-capability in order to be commercialized. Complex and costly material treatments of Sn have been effective in reducing capacity fade, but conventionally produced bare Sn is desired for reducing cost. One simple method is to form a high-quality solid electrolyte interphase (SEI) on Sn particles with low resistance and high passivation. Fluoroethylene carbonate (FEC) added to the electrolyte forms a protective and less-resistant SEI on Sn particles during the in-situ electrochemical SEI formation cycle. FEC is a good oxidizing agent that removes highly oxidized carbon compounds and makes a SEI thinner during an oxidation process (delithiation) of SEI formation cycle. The high-quality SEI greatly improves the rate-capability and capacity of nano-sized bare Sn electrodes without any treatments: minimal capacity fade (0.014% cycle^{-1}) at 320 mA h g^{-1} (1.3 C) for 150 cycles. The mitigating effect of FEC on capacity fade is not seen with electrodes fabricated from micro-scale (0.1∼0.2 μm) Sn. The long lithium-ion diffusion path makes these micro-sized materials susceptible to decrepitation during repeated volume changes.

*Corresponding author. Tel.: +1 404 747 0451.
E-mail addresses: keom@gatech.edu, kwangsup.eom@gmail.com (K. Eom).

http://dx.doi.org/10.1016/j.nanoen.2014.12.041
2211-2855/

Introduction

Li-ion batteries (LiBs) are the predominant energy storage system for electrical vehicles (EVs) as well as various consumer electronic devices. Their key attributes are long-term performance stability, good rate capability, and thermal stability in practical use [1-5]. However, one of the most critical challenges of the present commercial Li-ion batteries is insufficient capacity leading to a need for frequent charging. Hence, the development of new electrode materials with higher energy density is of significant interest [4].

Tin (Sn) is a promising material for the anode because Sn is inexpensive, naturally abundant, and has a high theoretical energy density (7260 mA h cm^{-3}) and specific energy [6,7]. In contrast to the intercalation of lithium in graphite, Sn forms an alloy with lithium. Alloying and de-alloying occur reversibly according to the following equation:

$$xLi + xe^{-} + Sn_y \leftrightarrow Li_xSn_y \quad (1)$$

For each Sn atom up to 4.4 Li ions are added ($Li_{22}Sn_5$ alloy), corresponding to a specific capacity of 992 mA h g^{-1}, which is 2.7 times higher than that of graphite ($\sim$372 mA h g^{-1}). Still, Sn and Sn based materials are difficult to commercialize due to severe capacity fading during battery cycling [7]. Similar to lithium-silicon systems, this fade is associated with the large volume expansion, up to 300%, when Sn is fully alloyed with Li [6-8]. Repeated alloying and de-alloying make Sn-based materials susceptible to pulverization, and concomitantly, the continuous formation of SEI compounds during cycling. This behavior leads to loss of cyclable lithium, consumption of electrolyte, and compromised electrical contact between particles, and hence, continuous capacity fading [7].

There have been many attempts to mitigate this capacity fade so that Sn can be used in a practical Li-ion battery; (i) Sn alloys, such as Sn-Ni [9-11], Sn-Cu [12], Sn-Co [13], Sn-Sb [14,15], (ii) Sn-carbon material composite, such as carbon coated Sn [8,16-20], Sn-CNT [21], and Sn-graphene [22-26], (iii) structural modification, such as nano-scaled Sn on nanomaterial [27-29] and hollow- [30,31]/cube-shaped Sn [32], and (iv) combinations of (i)-(iii) [8,27-32]. Among them, several efforts were encouraging: high capacity, high rate-capability, and low capacity fade. However, compared to graphite, the fabrication processes of modified Sn and Sn based alloy materials are complex and expensive, representing a barrier to commercialization. Specifically, the key obstacles are poor reproducibility, low production yields, low rates of production, and safety hazards [16,20]. Hence, to spur commercialization, electrode materials that use Sn without complex treatments while still retaining high stability and good rate-capability are needed.

Herein, we report on the formation of a robust solid electrolyte interphase (SEI) that protects against pulverization and where the SEI is formed for the most part only during the first electrochemical cycle. The process is referred to 'in-situ electrochemical SEI formation cycle' in this paper. A high-quality SEI is needed to maintain high performance, and it should be uniform, adhere well to the negative electrode, and have high ionic and electronic conductivities [33-35]. The SEI is formed from the reduction and polymerization of the electrolyte solvents. Additives to the electrolyte can improve the quality and composition of SEI [36-39]. In particular, fluoro-ethylene carbonate (FEC) has been shown to be effective in reducing irreversible capacity loss and lowering capacity fade for several carbon and silicon based anode materials [36-38,40,41]. The effects of the FEC additive on SEI properties of bare Sn electrode and the formation and degradation mechanisms of the SEI on Sn anode are not yet fully understood.

In this context, we synthesized nano- and micro-sized bare Sn materials for use in a lithium ion battery and investigated their electrochemical and morphological properties with and without FEC as an electrolyte additive. Specifically, the formation and degradation mechanisms of nano-/micro-scaled Sn electrodes with different qualities SEI were scrutinized.

Results and discussion

In this study, two sizes of Sn material, nano- (5$\sim$10 nm) and micro (0.1$\sim$0.2 μm)- scaled spherical particles, were synthesized by chemical reduction methods. The electron microscopy images of the synthesized Sn particles are shown in Figure S1. To assess the electrochemical properties of the synthesized Sn particles with and without FEC additives, coin-cells were prepared and tested. Four variants were studied (i) micro-sized Sn with FEC, (ii) nano-sized Sn with FEC, (iii) nano-sized Sn without FEC, and (iv) micro-sized Sn without FEC. The electrochemical performance of type (iv) was too poor to compare directly to the other cells, and thus it will not be discussed further.

Figure 1 shows the electrochemical performance of the three cells. In the electrochemical SEI formation cycle (Figure 1a), the theoretical Sn capacity during the first lithiation was exceeded due to other reduction reactions associated with the SEI formation. There were oxides of Sn that remained on the surface from the synthesis process. These oxides react to form SEI compounds, such as Li oxides, and thereby increase the charge that must be passed during the first lithiation of the tin. From the XRD patterns of Figure S2, it was confirmed that Sn oxides completely disappeared after the first cycle. In Figure 1a, it is notable that Sn electrodes with FEC have a lithiation capacity 150 mA h g^{-1} (10.6%) less than the electrode without FEC. This result was observed for both micro- and nano-sized particles, suggesting that FEC impedes the excess SEI formation leading to less exhaustion of Li ions during the first reduction process. During subsequent delithiations, the nano-Sn electrode with FEC has 19.9% and 14.0% higher capacity than nano-Sn electrode without FEC and micro-Sn electrode with FEC, respectively.

As shown in rate-capability and stability tests of Figure 1b, the nano-Sn electrode with FEC exhibited the highest rate-capability during electrochemical cycling between 0.01 V and 1.5 V. The micro-sized Sn electrode showed the lowest rate-capability and very poor cyclability at any lithiation/delithiation rate greater than 160 mA g^{-1}. Material fracture was suspected as the cause for the high capacity fade, presumably due to the repeated non-uniform dilation and contraction during alloying and de-alloying. The characteristic time for diffusion of lithium in the solid phase scales with the

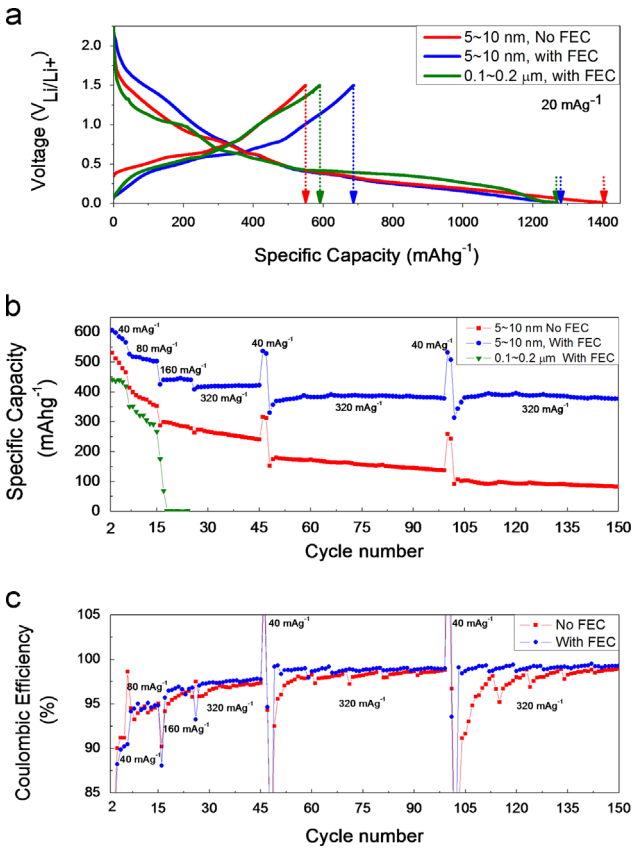

Figure 1 Electrochemical performance of micro-/nano-sized Sn electrodes with/without FEC electrolyte additive. (a) In-situ electrochemical SEI formation cycle (first lithiation and delithiation process at extremely slow rate of 20 mA g^{-1}); (b) delithiation capacity as a function of cycle number for estimation of rate-capability (at various current densities) and capacity fade (at 320 mA h g^{-1} (1.3 C)); (c) coulombic efficiency during cycling.

square of the particle size ($\tau \sim \ell^2$). For the micron-sized particles the characteristic time is about 400 times larger than for the nano-particles. When the diffusion time is large compared to the discharge time, uneven lithiation and delithiation states (different phases with different mechanical strengths) inside one particle results. These variations in composition lead to stress, which can lead to crack propagation and pulverization. Indeed, fractures and crack propagation were observed in the SEM images (Figure S3) of cycled micro-Sn electrodes, which exhibited poor electrochemical performance.

Nano-sized Sn without FEC showed continuous capacity fade at a current density between 40 and 320 mA g^{-1}, whereas the nano-Sn electrode with FEC showed a decrease in capacity during initial 10 cycles at 40 and 80 mA g^{-1}due to initial stabilization, but no decay after 10 cycles even at higher current densities of 160 (11 to 24 cycle) and 320 mA g^{-1} (after 25th cycle) to a test end (for postmortem analysis).

When comparing the 40 mA g^{-1} capacity of 45th cycle to 100th cycle, it was found that the electrode without FEC decreased by 22.7% (0.41% $cycle^{-1}$), whereas with FEC the capacity fade was minimal (0.014% $cycle^{-1}$). It indicated that in terms of actual capacity loss, the electrode with FEC has less degradation than that without FEC. From the columbic efficiency of Figure 1c, it is evident that FEC stabilizes the lithiation and delithiation behavior of the nano-Sn electrode. To the best of our knowledge, this amount of improvement of bare Sn electrode without any material treatments even without carbon coating has not been reported. The Sn electrode had no decay of capacity at 320 mA h g^{-1} (1.3 C) to 150 cycle, especially in 150 cycle, 260% higher capacity than Sn electrode with general SEI without FEC. Hence, it is necessary to elucidate the mechanism on the effect of FEC on the nano-Sn electrode.

In this work, the SEI formation cycle was methodically investigated electrochemically using differential capacity (dC/dV). In addition, the composition and morphology of the surface were examined with XPS and HR-TEM, as shown in Figure 2. The dissimilar behavior between the nano-Sn electrodes with and without FEC is illustrated clearly by the differential-capacity curves. During the first lithiation process, the Sn electrode without FEC showed many relatively large peaks (more negative) between 0.45 $V_{Li/Li+}$ and 0.01 $V_{Li/Li+}$. In contrast, with FEC the lithiation peaks were smaller (less negative). During delithiation, the first peak, representing the start of lithium removal, was observed to be at about 0.41 V without FEC compared to a potential of 0.11 V with FEC. In particular, the initiation of delithiation at a lower potential suggests more facile movement of Li ions from Li_xSn_y alloy to electrolyte, which is directly related with lower irreversible capacity loss (ICL), presented in Figure 2a. To elucidate the SEI formation and stabilization mechanism of Sn electrode with FEC, XPS and HR-TEM analyses were conducted on the pristine electrode as well as on those with varied states of lithiation: fully lithiated (0.01 $V_{Li/Li+}$), partial lithiation (at 0.45 $V_{Li/Li+}$), and fully delithiated (at 1.5 $V_{Li/Li+}$). Figure 2b shows the XPS peaks between binding energy of 292.0 and 282.0 eV for the carbon 1s orbital. The pristine nano-Sn electrode has only a peak at 284.5 eV corresponding to C-C single bonding of carbon black. However, when lithiated to 0.45 V, this peak disappears. Several new peaks are observed at higher binding energies of 285.0, 286.5, and 291.0 eV. These peaks correspond to C-O, O-C=O, and -R-CH_2OCO_2Li/-Li_2CO_3 compounds, respectively. After the full lithiation, many peaks were detected between 285.5 and 291.0 eV corresponding to C=O, O-C=O, CH_2OCO_2Li, and Li_2CO_3 (C=O: 286-287 eV, O-C=O: 289.0 eV, -R-CH_2OCO_2Li: 288-289 eV, -Li_2CO_3: 290 eV, -R-CH_2OCO_2Li: 290-291 eV [33,37,42]). The peaks with higher binding energies (288-291 eV), which correspond to highly oxidized carbon compounds, decreased dramatically during the subsequent delithiation. Only two peaks of 285.0 (C-O) and 286.5 eV (C=O) in low-binding energy region were detected. In contrast, the XPS spectra for the nano-Sn electrode without FEC still showed a large peak at a high binding energy of 288-291.0 eV (corresponding to highly oxidized carbon compounds), similar to that of fully lithiated state. Accordingly, it was found that FEC is a good oxidizing agent to remove highly oxidized SEI compounds, and it would promote the formation of a thinner SEI with lower resistance for Li ion diffusion and electron transfer.

To observe directly SEI on individual Sn particles during the first formation cycle, high magnification bright-field images using HR-TEM were obtained at the same potentials used for the XPS study as shown in Figure 2c. The relatively

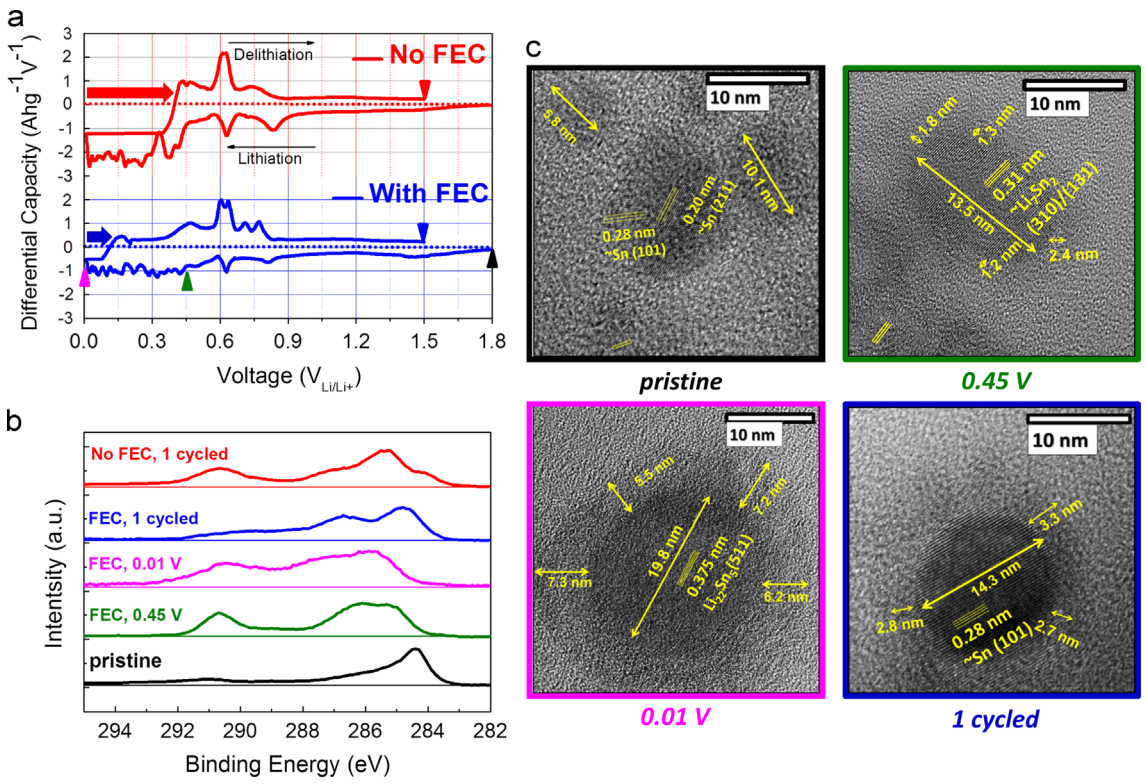

Figure 2 Formation mechanism of high-quality SEI on nano-Sn material with FEC during in-situ electrochemical SEI formation cycle (a) differential capacity curve versus voltage ($V_{Li/Li+}$) of nano-Sn electrode with/without FEC additive during 1st formation cycle; (b) XPS C1s peaks during 1st formation cycle; (c) high-magnification HR-TEM images (10 nm scale bar) of nano-Sn particles before, during lithiation (at 0.45 V and 0.01 V), and after delithiation (1st cycled states).

lower magnification images showing the distributions and average sizes of particles are in Figure S4. The diameters of pristine nano-Sn particles vary from 5.8 to 10.1 nm (avg: 6.9 nm). These Sn particles have a lattice parameters of 0.28-0.20 nm for the (101) and (211) planes respectively. When lithiated to 0.45 V, the size in the long direction of one specific particle increased to 13.5 nm (avg: 9.1 nm). The lattice parameter was measured to be 0.31 nm, corresponding to (310) and (131) planes of Li_7Sn_2. The average size of particles increased by 32%, and it was confirmed that an outer layer appeared along the surface of LiSn alloy particles with a thickness of 1.3~2.4 nm. When fully lithiated (0.01 V), one specific particle expanded by a large amount to 19.8 nm (avg: 14.5 nm). On the basis of the lattice parameter (0.375 nm) corresponding to (511) plane of $Li_{22}Sn_5$, this particle was considered to be fully lithiated to $Li_{4.4}Sn$. The thickness of SEI increased to 5.5~7.3 nm, and the layer appears much clearer than the one observed at 0.45 V. The improved contrast is because the SEI is composed of various kinds of organic, inorganic, and carbonate groups that are highly oxidized as confirmed in XPS of Figure 2b. After the subsequent delithiation, however, the average sizes of particles decreased to 9.7 nm, but still 19.6% larger than those of the pristine particles. It might be because all Sn particles were not fully delithiated and voids and defects were produced during the first cycle. Then, the SEI became thinner to 2.7~3.3 nm, but thicker than that of 0.45 V, which has fully covered the entire surface to impede direct attack of electrolyte to bare Sn.

The interpretation of the electrochemical impedance spectra (Figure S5) is consistent with the above XPS and HR-TEM results. On the Nyquist plot, the first feature observed at high frequencies is attributed to the SEI layer and represents the SEI resistance, R_{SEI}. After the first lithiation, the SEI resistances of both cells are similar as 26.3 and 32.1 $\Omega\,cm^2$ with and without FEC, respectively. Following the subsequent delithiation, however, the difference was clear; the SEI resistance of the Sn electrode with FEC decreased by 48.4%, compared to a reduction of 15.2% without FEC. This difference suggests that during the 1st delithiation the SEI for nano-Sn is stabilized with FEC [43]. Based on the above results (Figures 2 and S5), it is notable that FEC promotes the thin but low-resistance SEI on nano-Sn particles. The improved SEI is hypothesized to be attributed to the removal (on subsequent delithiation) of highly oxidized carbon compounds formed during the 1st lithiation. The formation of this high-quality SEI can increase the rate-capability and cycle stability of bare Sn electrode without additional material treatments such as carbon coating and structural modification.

Figure 3 compares postmortem analyses of cycled nano-Sn electrode with and without FEC additive using XPS and HR-TEM. The intensities of peaks near 290.0~291.5 eV and 286.5 eV, which correspond to organic/carbonate compounds and C=O bonding [33,37,42], respectively, increased significantly without FEC. On the other hand, with FEC the peaks at high binding energies increased slightly, and the other peaks at low binding energies remained constant compared to Figure 2b based on C-O peak of 285.0 eV [33,37,42].

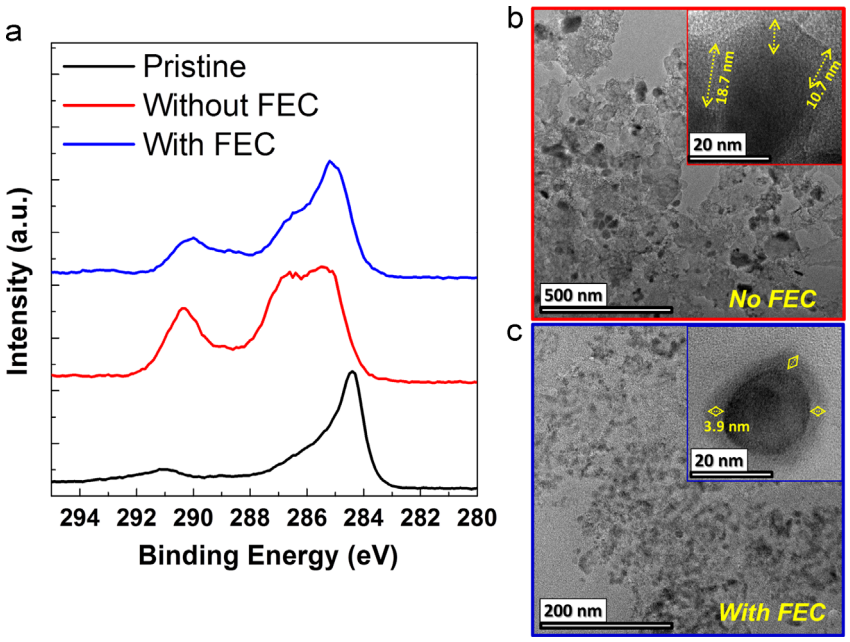

Figure 3 Postmortem XPS and HR-TEM analyses of nano-sized Sn electrodes with/without electrolyte additive of FEC. (a) C1s XPS of pristine and cycled Sn electrode; (b) HR-TEM images (low/high magnification) of cycled Sn electrode without FEC; (c) with FEC additive.

Lower-magnification HR-TEM images clearly show differences in the cycled Sn electrodes with and without FEC additive. Even with lower magnification, the Sn electrode without FEC has a few agglomerated large particles (dark spots) and a larger amount of bright matrix mostly from accumulated SEI compounds. The Sn electrode with FEC exhibited well-distributed Sn nano-particles and a smaller amount of bright matrix even after cycling. In the high magnification images, which show individual Sn particles, the nano-Sn electrode without FEC has thick and uneven SEI of 10.7∼18.7 nm, whereas with FEC the Sn particle has a uniform SEI of about 3.9 nm even after cycling. The above results plainly elucidate the reasons why nano-Sn particles with FEC have good stability and high rate-capability during long-term cycling. In Figure S6, the medium-magnification HR-TEM images reveal the distribution and average sizes of the Sn particles from cycled nano-Sn electrodes with/without FEC. The Sn particles with FEC were well-distributed relatively compared to those without FEC; the sizes are about half and the particles less agglomerated due to stable protection by a more uniform SEI. The EIS data, shown in Figure S5, support the above postmortem results. After cycling, the SEI resistance of nano-Sn electrode increased 3.4 times, while that with FEC increased by 1.5 times, indicating that FEC is effective in mitigating an increase in SEI resistance during long-term cycles by forming stable SEI initially.

On the basis of the results in Figures 1–3and S1–S6, the SEI formation and degradation mechanims of Sn electrode, which are affected by particle size and FEC additive, can be clearly proposed. Figure 4 shows schematic of the two dimensional cross-sectional images of 1st lithiated, 1st delithiated, and cycled micro-/nano-Sn particles with/without electrolyte additive to form thin and protective SEI.

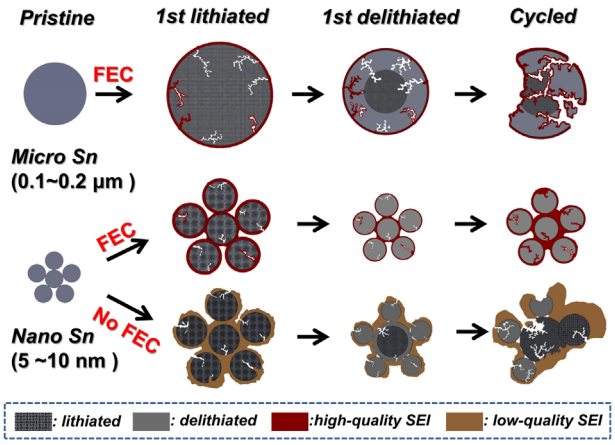

Figure 4 Schematic of the formation and degradation mechanisms of micro-/nano-scaled Sn particles with high/low-quality SEI, showing the two dimensional cross-sectional images of 1st lithiated, 1st delithiated, and cycled micro-/nano-Sn particles with/without FEC electrolyte additive. This schematic is based on HR-TEM/SEM images and XPS data of Figures 2b and c, 3, and S4 and S6. Micro-Sn particle has long lithium ion diffusion path and easy mechanical fraction by continuous crack propagation from repeated expansion/contraction although thin and protective SEI is formed by FEC electrolyte additive. Nano-Sn particles with FEC additive form high-quality SEI on surface, and have low degradation during cycling due to short Li diffusion path, low SEI resistance, and tight protection from electrolyte attack. In contrast, nano-sized Sn particles with low quality SEI (without FEC) are unprotected from mechanical fractures and chemical attack, and then have loss of particle and film resistance increases continuously during cycling.

During the first lithiation, micro-Sn particles expand by a large amount, SEI is produced along the surface of particles, and cracks are produced due to increased tensile stress. When delithiated, long diffusion path of micro-particle and formed SEI outside of the particle allow some Li ions (especially, inside LiSn alloy far from outside) to be confined inside the particle at a specific rate, and the cracks are propagated due to highly induced compressive stress. The repeated lithiation and delithiation processes make continuous crack propagation leading to pulverization of particles. SEI compounds are formed repeatedly on newly exposed surface created by pulverization, resulting in loss of cyclable lithium and electrolyte. Consequently, micro-particles degradaded easily due to long diffusion distance and low mechanical toughness regardless of FEC addition to form protective SEI; that is, FEC cannot impede decrepitation.

In contrast, because nano-sized Sn particles less than 10 nm in diameter have short-diffusion paths for lithium ions, they have high intrinsic rate-capability and lower mechanical stress from deforming. Upon initial lithiation, nano-Sn particles expand and SEI is produced along the surface of particle and between particles. Then, the properties of formed SEI determine the cycle life of nano-Sn particles. Nano-Sn particles with FEC form a high-quality SEI. Thus these cells retain high stability and rate capability due to low SEI resistance, and the better protection of active materials from continuous attack of electrolyte by forming a thin and chemically stable SEI.

However, the nano-Sn particles that form thicker and less conductive SEIs during first SEI formation cycle, have relatively poor rate capability, and then irregular state of lithiation (different lithium–tin alloy phases) inside one particle. Due to different mechanical strengths of different phases, cracks would be easily propagated and then cause particle to be fractured. The repetition of this behavior leads to continuous capacity loss along with decay of rate-capability.

Conclusions

Nano- and micro-scaled bare Sn materials for lithium ion battery were synthesized by chemical methods, and their electrochemical and morphological properties with and without FEC additive for lithium ion battery were investigated. Specifically, the formation and degradation mechanisms of bare nano-/micro-scaled Sn electrodes with protective SEI by FEC additive were scrutinized. From the high magnification images of HR-TEM and XPS analyses during in-situ electrochemical SEI formation cycle, it was found that FEC played a role of a good oxidizing agent to promote to removal of SEI with highly oxidized carbon compounds (with high binding energy) during an oxidation process (delithiation); high-quality SEI with thin and low resistance improved greatly the rate-capability and capacity of bare of nano-sized bare Sn electrodes, which was synthesized by a conventional method without special material treatment and even no carbon-coating. The Sn electrode had no decay of capacity at 320 mA h g^{-1} (1.3 C) to 150 cycle and more, especially in 150 cycle, 260% higher capacity than Sn electrode with general SEI without FEC. On the other hand, the micro-scale (0.1∼0.2 μm) Sn electrode did not benefit from the FEC addition due to long lithium ion diffusion path and the susceptibility to fracture during the repeated volume changes.

For future feasibility tests of commercialization of this bare Sn electrode with a robust SEI, full-cells employing various types of commercial electrodes, such as layered lithium nickel cobalt manganese oxide (NCM) and spinel lithium manganese oxide (LMO) and olivine lithium iron phosphate (LFP), will be designed and tested, and the amount of FEC will be optimized.

Experimental methods

Synthesis of micro-/nano-sized Sn particles

Both-types of spherical Sn particles, with nano- (5∼10 nm) and micro (0.1 ∼0.2 μm)-in diameter, were prepared via a chemical reduction method by a modified literature method [22,44]. Specifically, tin (IV) chloride ($SnCl_4$, Aldrich) and trisodium citrate dehydrate ($HOC(COONa)(CH_2COONa)_2 \cdot 2H_2O$, Aldrich) were used as Sn source and capping agent, respectively. The reactants were fully dissolved in ethylene glycol (EG, $C_2H_6O_2$, Aldrich) by agitating with a stirring bar at 1000 rpm, followed by the addition of the reducing agent, sodium borohydride ($NaBH_4$, Aldrich). The molar ratio between $SnCl_4$ and $NaBH_4$ was 1:50 and 1:10 for nano- and micro-sized Sn particles, respectively. After 5 min of reaction, the synthesis reactions were done. Afterward, the products were washed using methanol (CH_3OH, 99.8% purity, Aldrich) and deaerated deionized water, and then collected by centrifugation at 10,000 rpm for 10 min. After 5 times of the washing and filtering process, the collected wet Sn powder was dried at 120 °C under vacuum (below 10^{-3} Torr) for 24 h. The produced Sn particle had >95.0 wt% purity (3∼4 wt% byproduct composed of C and N) by EDS analysis except for oxygen contents. The two types of solvent make the size difference of spherical Sn particles in this process. The Sn particles produced in EG were 0.1∼0.2 μm in diameter, whereas those in DMF were in 5∼10 nm. The surface morphologies and compositions of synthesized Sn particles are in Figure S1.

Preparation of Sn electrodes and cell assembly

To make the slurry of adhesive and conductive Sn anode material, the nano-/micro-sized active Sn material of 80 wt% was combined with polyvinylidenefluoride (PVdF) binder ($(-(C_2H_2F_2)_n-$, M_v: 450,000 g mol^{-1}, Sigma Aldrich) of 10 wt%, carbon black conductive agent (Super C65, TIMCAL,) of 10 wt %, and NMP solvent (N-Methyl-2-pyrrolidone, Sigma Aldrich) of 15 ml/g. After mixing the slurry by sonication and stirring with magnetic bar in a jar, the slurry was coated on a 10 μm Cu foil using a doctor blade. The slurry coated on Cu foil was dried for 1 h at a room temperature and then in a vacuum oven of 120 °C overnight. Using the completed Sn electrode as the working electrode, coin-type half-cells (2032) were assembled. The electrolyte used in the half-cells was EC: DEC=1:1 (wt%) with 1 M $LiPF_6$ with/without FEC additive (the content should be optimized for the best electrochemical performance [40]). A microporous trilayer membrane (Celgard 2325) was used as a separator, and the electrolyte of 75 μl was applied for one coin cell.

Electrochemical tests

To characterize the electrochemical properties of the fabricated Sn electrodes, capacity-voltage (*C-V*) tests and Electrochemical Impedance Spectroscopy (EIS) test were performed. All cycling tests were conducted at room temperature (~20 °C) using an Arbin battery cycler. The half-cells were charged to 1.5 V and discharged to 0.01 V (1 h rest time between charge and discharge) at various rates from 20 mA g^{-1} for in-situ SEI formation cycle (first cycle) to 340 mA g^{-1} (~1.3 C) for capacity fade test cycling. EIS tests of the Sn electrodes were conducted at both a nearly full lithiated of 0.1~0.15 V (OCV) and the fully delithiated state of 1.05~1.10 V (OCV) using a potentiostat (Autolab). The frequency was scanned from 1 MHz~0.01 Hz using a 5 mV amplitude perturbation. The values for resistances of individual components were determined with a fitting program (Gamry Echem Analyst).

Material characterization

For material characterization during and after electrochemical test, the cells were opened in an Ar-filled glove box and washed gently for 2 min in extra pure dimethyl carbonate (DMC, $C_3H_6O_3$, Aldrich) to remove Li salts fully, and the samples were stored in containers filled with Ar before analysis to prevent any contact with air. To observe the surface morphology, phases, and atomic compositions of nano-sized (5~10 nm) Sn particles, High Resolution (HR)-Transmission Electron Microscope (TEM) equipped with Energy Dispersive X-ray spectroscopy (EDS) (FEI Tecnai F30, 300 kV) was used. Using the HR-TEM, bright-field images, EDS line scanning (in STEM mode), and diffraction patterns were obtained. To examine the chemical composition of SEI, X-ray photoelectron spectroscopy (Kratos XPS) analysis was performed. In addition, X-ray diffraction (XRD, X'Pert PRO Alpha-1) and HR-scanning electron microscopy (HR-SEM, Hitachi SU8000) and SEM/EDS (Zeiss Leo 1530) and Focused Ion Beam (FIB)-SEM (FEI Nova nanolab 200) were used to observe phases, crystallinity, compositions, and cross-sectional morphology of materials (Supporting Information).

Acknowledgment

This research was supported by the School of Chemical & Biomolecular Engineering and Center for Innovative Fuel Cell and Battery Technologies of Georgia Institute of Technology.

Appendix A. Supporting information

Supplementary data associated with this article can be found in the online version at http://dx.doi.org/10.1016/j.nanoen.2014.12.041.

References

[1] M. Winter, J.O. Besenhard, M.E. Spahr, P. Novák, Adv. Mater. 10 (1998) 725-763.
[2] M.S. Whittingham, Chem. Rev. 104 (2004) 4271-4302.
[3] F. Cheng, J. Liang, Z. Tao, J. Chen, Adv. Mater. 23 (2011) 1695-1715.
[4] V. Etacheri, R. Marom, R. Elazari, G. Salitra, D. Aurbach, Energy Environ. Sci. 4 (2011) 3243-3262.
[5] M. Armand, J.M. Tarascon, Nature 451 (2008) 652-657.
[6] D. Larcher, S. Beattie, M. Morcrette, K. Edstrom, J.-C. Jumas, J.-M. Tarascon, J. Mater. Chem. 17 (2007) 3759-3772.
[7] B. Wang, B. Luo, X. Li, L. Zhi, Mater. Today 15 (2012) 544-552.
[8] Y. Xu, Q. Liu, Y. Zhu, Y. Liu, A. Langrock, M.R. Zachariah, C. Wang, Nano Lett. 13 (2013) 470-474.
[9] K.K.D. Ehinon, S. Naille, R. Dedryvère, P.E. Lippens, J.C. Jumas, D. Gonbeau, Chem. Mater. 20 (2008) 5388-5398.
[10] J. Hassoun, S. Panero, P. Simon, P.L. Taberna, B. Scrosati, Adv. Mater. 19 (2007) 1632-1635.
[11] R. Hu, H. Liu, M. Zeng, H. Wang, M. Zhu, J. Mater. Chem. 21 (2011) 4629-4635.
[12] H.C. Shin, M. Liu, Adv. Funct. Mater. 15 (2005) 582-586.
[13] X.J. Zhu, Z.P. Guo, P. Zhang, G.D. Du, R. Zeng, Z.X. Chen, S. Li, H.K. Liu, J. Mater. Chem. 19 (2009) 8360-8365.
[14] Y. Wang, I. Djerdj, B. Smarsly, M. Antonietti, Chem. Mater. 21 (2009) 3202-3209.
[15] C.-M. Park, K.-J. Jeon, Chem. Commun. 47 (2011) 2122-2124.
[16] G. Derrien, J. Hassoun, S. Panero, B. Scrosati, Adv. Mater. 19 (2007) 2336-2340.
[17] M. Mouyane, J.M. Ruiz, M. Artus, S. Cassaignon, J.P. Jolivet, G. Caillon, C. Jordy, K. Driesen, J. Scoyer, L. Stievano, J. Olivier-Fourcade, J.C. Jumas, J. Power Sour. 196 (2011) 6863-6869.
[18] W. Li, R. Yang, J. Zheng, X. Li, Nano Energy 2 (2013) 1314-1321.
[19] Y. Xu, Y. Zhu, Y. Liu, C. Wang, Adv. Energy Mater. 3 (2013) 128-133.
[20] J. Hassoun, G. Derrien, S. Panero, B. Scrosati, Adv. Mater. 20 (2008) 3169-3175.
[21] Y. Wang, M. Wu, Z. Jiao, J.Y. Lee, Chem. Mater. 21 (2009) 3210-3215.
[22] G. Wang, B. Wang, X. Wang, J. Park, S. Dou, H. Ahn, K. Kim, J. Mater. Chem. 19 (2009) 8378-8384.
[23] L. Ji, Z. Tan, T. Kuykendall, E.J. An, Y. Fu, V. Battaglia, Y. Zhang, Energy Environ. Sci. 4 (2011) 3611-3616.
[24] B. Luo, B. Wang, X. Li, Y. Jia, M. Liang, L. Zhi, Adv. Mater. 24 (2012) 3538-3543.
[25] X. Zhou, L.-J. Wan, Y.-G. Guo, Adv. Mater. 25 (2013) 2152-2157.
[26] N. Li, H. Song, H. Cui, C. Wang, Nano Energy 3 (2014) 102-112.
[27] Z. Yang, G. Du, Q. Meng, Z. Guo, X. Yu, Z. Chen, T. Guo, R. Zeng, RSC Adv. 1 (2011) 1834-1840.
[28] Y. Yu, L. Gu, X. Lang, C. Zhu, T. Fujita, M. Chen, J. Maier, Adv. Mater. 23 (2011) 2443-2447.
[29] F.-S. Ke, L. Huang, L. Jamison, L.-J. Xue, G.-Z. Wei, J.-T. Li, X.-D. Zhou, S.-G. Sun, Nano Energy 2 (2013) 595-603.
[30] S. Ding, J.S. Chen, G. Qi, X. Duan, Z. Wang, E.P. Giannelis, L.A. Archer, X.W. Lou, J. Am. Chem. Soc. 133 (2010) 21-23.
[31] X.W. Lou, Y. Wang, C. Yuan, J.Y. Lee, L.A. Archer, Adv. Mater. 18 (2006) 2325-2329.
[32] L. Zhang, H.B. Wu, B. Liu, X.W. Lou, Energy Environ. Sci. 7 (2014) 1013-1017.
[33] M. Lu, H. Cheng, Y. Yang, Electrochim. Acta 53 (2008) 3539-3546.
[34] W.R. Liu, J.H. Wang, H.C. Wu, D.T. Shieh, M.H. Yang, N.L. Wu, J. Electrochem. Soc. 152 (2005) A1719-A1725.
[35] Y.M. Kang, J.Y. Go, S.M. Lee, W.U. Choi, Electrochem. Commun. 9 (2007) 1276-1281.
[36] V. Etacheri, O. Haik, Y. Goffer, G.A. Roberts, I.C. Stefan, R. Fasching, D. Aurbach, Langmuir 28 (2011) 965-976.
[37] H. Nakai, T. Kubota, A. Kita, A. Kawashima, J. Electrochem. Soc. 158 (2011) A798-A801.

[38] Y.-M. Lin, K.C. Klavetter, P.R. Abel, N.C. Davy, J.L. Snider, A. Heller, C.B. Mullins, Chem. Commun. 48 (2012) 7268–7270.
[39] S.S. Zhang, J. Power Sour. 162 (2006) 1379–1394.
[40] A. Bordes, K. Eom, T.F. Fuller, J. Power Sour. 257 (2014) 163–169.
[41] K. Eom, T. Joshi, A. Bordes, I. Do, T.F. Fuller, J. Power Sour. 249 (2014) 118–124.
[42] A.M. Andersson, A. Henningson, H. Siegbahn, U. Jansson, K. Edström, J. Power Sour. 119–121 (2003) 522–527.
[43] S.S. Zhang, K. Xu, T.R. Jow, Electrochim. Acta 51 (2006) 1636–1640.
[44] M. Noh, Y. Kwon, H. Lee, J. Cho, Y. Kim, M.G. Kim, Chem. Mater. 17 (2005) 1926–1929.

KwangSup Eom is a postdoctoral fellow at the Georgia Institute of Technology. He received his B.S., M.S., and Ph.D in Materials Science and Technology (MSE) from KAIST. His Ph.D study focused on the hydrogen production and storage using chemical hydrides and metal alloys, based on electrochemical catalysis and corrosion. From August 2010 to November 2012, he studied the electrochemical degradation (corrosion) mechanism of PEM fuel cells, and developed non-noble catalysts at the Fuel Cell Research Center of KIST. His current research interests include new material development and electrochemical mechanism study for next generation energy storage and production system of battery and fuel cell.

Jaehan Jung received the B.S. degree in Materials Science and Engineering from the Seoul National University, Republic of Korea in 2010. He is currently a Ph.D. candidate in Materials Science and Engineering at the Georgia Institute of Technology studying under Prof. Zhiqun Lin. His current research interests include inorganic-organic nanocomposites and their application in optoelectronic devices and batteries.

Jung Tae Lee is a postdoctoral research scholar at the Georgia Institute of Technology. He received his B.S. in Food Science and Technology (Division of Life Biotechnology) and B.B.A. in Global Management from the Kyunghee University in 2008, and M.S. in Materials Science and Engineering from the Seoul National University in 2010. He earned his Ph.D. in Polymer Textile and Fiber Engineering (School of Materials Science Engineering) at the Georgia Institute of Technology in 2014. His current research focuses on developing novel nanomaterials and their composites with structure controls at nanoscale for advanced Li-ion and next generation batteries.

Valentin Lair is an undergraduate student in a Master of Electrochemical and Process Engineering, at the Phelma – Grenoble Institute of Technology, France. In 2014, he was a visiting student in Professor Tom Fuller's group at the Georgia Institute of Technology. His main research experience concerns new material development for lithium ion batteries.

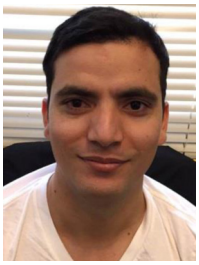

Tapesh Joshi is a graduate student in the School of Chemical & Biomolecular Engineering (ChBE) at the Georgia Institute of Technology. He received his undergraduate degree in Chemical Engineering from the Brigham Young University. He is being advised by Thomas F. Fuller in ChBE Department and Gleb Yushin in Material Science & Engineering Department. His research focuses on understanding degradation mechanisms in lithium-ion batteries.

Dr. Seung Woo Lee is an assistant professor of the Woodruff School of Mechanical Engineering at the Georgia Institute of Technology. Dr. Lee has expertise in electrode materials and electrochemical measurement techniques for energy storage and conversion devices, including rechargeable batteries, supercapacitors, fuel-cells, and electrolyzers. Dr. Lee has focused on studying surface chemistry and electronic structure of various electrode materials, such as carbon nanotubes, graphenes, and metal (oxide) nanoparticles, correlating with their electrochemical properties.

Zhiqun Lin is a Professor in the School of Materials Science and Engineering at the Georgia Institute of Technology. He received his Ph.D. in Polymer Science and Engineering from the University of Massachusetts, Amherst in 2002. His research interests include perovskite solar cells, polymer solar cells, dye-sensitized solar cells, semiconductor organic-inorganic nanocomposites, photocatalysis, lithium ion batteries, quantum dots (rods), conjugated polymers, block copolymers, polymer blends, hierarchical structure formation and assembly, surface and interfacial properties, multifunctional nanocrystals, and Janus nanostructures.

Thomas Fuller is a Professor of Chemical & Biomolecular Engineering at the Georgia Institute of Technology, where he co-directs the GT Center for Innovative Battery and Fuel Cell Technologies. In 2007 he received the Energy Technology Division Research Award of the Electrochemical Society and is a Fellow of the Electrochemical Society.